29

Royal Norwegian Council for Scientific and Industrial Research

ONE ARRAY AND TWO ARRAY LOCATION CAPABILITIES

by

H. Gjøystdal, E. S. Husebye and
D. Rieber-Mohn

June, 1972

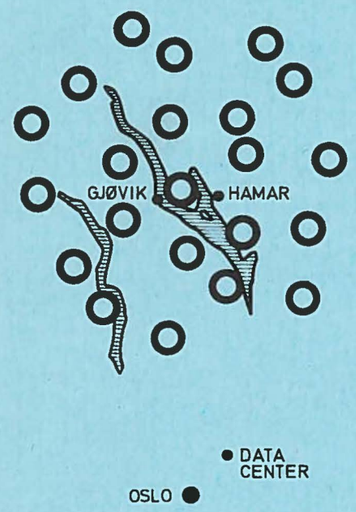

NORWEGIAN SEISMIC ARRAY

NORSAR

P. O. Box 51. 2007 Kjeller – Norway

NTNF/NORSAR
P. O. Box 51 - 2007 Kjeller
Norway

NORSAR Report No 29

ONE ARRAY AND TWO ARRAY LOCATION CAPABILITIES

by

H. Gjøystdal, E. S. Husebye and
D. Rieber-Mohn

June, 1972

The NORSAR research project has been sponsored by the United States of America under the overall direction of the Advanced Research Projects Agency and the Technical management of the Electronic System Division, Air Force System Command, through Contract No. F19628-70-C-0283 with the Royal Norwegian Council for Scientific and Industrial Research.

INTRODUCTION

Several methods have been developed for locating seismic events, and the precision in the final epicenter parameters depends on the location algorithm, number of stations used, observational errors and heterogeneities in the Earth itself. Obviously, the best estimate of the epicenter coordinates is obtained by using data from a large number of stations having a reasonable distribution in distance and azimuth from the source (e.g. Bolt, 1960). On the other hand, Evernden (1969) has demonstrated that very precise event locations are possible by restricting the observational data to accurately calibrated P-arrival times from a few stations.

A new dimension to the location of seismic events is represented by the large aperture seismic arrays like LASA and NORSAR. These stations both detect and locate many events which are left unreported by an organization like NOAA (previously USCGS). We have investigated the above problem emphasizing the estimate of 95% confidence ellipses for event locations based on data from one or two arrays. The latter restriction is introduced as the LASA and NORSAR arrays have a direct communication link for mutual data exchange. Moreover, we have chosen whenever possible a quite general approach to the above problem, i.e. a simulation on the computer of the array location process in terms of random and biased errors in the observational data like arrival time, azimuth and velocity of the incoming wavefront. This implies that the arrays are represented in terms of the observational precision in the above parameters and not as a function of aperture and number of sensors in use.

differences between phases like PKIKP and PKP are available. Considering the spherical triangle whose corners are the North Pole, the array center and the event location (see Fig 1a), we are now in a position to compute the latitude and longitude of the epicenter. The basic trigonometric equations for spherical triangles are given in many standard textbooks and henceforth omitted. In order to simulate the event location capability of one array we proceed as follows:

The first step is to obtain a random Gaussian distribution of the parameters azimuth and slowness (DT/DΔ). Specifying their mean values and variances 200 paired values of these two parameters are simulated by using a random number generation routine. These observations determine a distribution of event locations in geographic space, each point having a unique latitude and longitude. Actually, we are pointing the array towards a specified point on the earth which for computational convenience is located on the equator, i.e., o.o. N and o.o E. In other words, when dealing with different epicentral distance intervals, the event locations are always restricted to the equatorial area while the fictive array may be moved northwards in steps of say 10 deg as actually used (see Fig 2). The simulated epicenters are considered in a Carthesian coordinate system, the X and Y axis pointing east and north. Thus, having obtained a point distribution in this rectangular system, we calculate the axes of the 95% confidence ellipse using a method described by Evernden (1969). It should be noted that a one-to-one transformation between geographic and Carthesian space is used, an approximation which is justified in view of the small areas covered by the event locations in question.

generation routine, the desired event location population is easily created. As before, we can determine the point distribution in geographic space and then the probability surface which give the axes and orientation of the 95% confidence ellipse (see Fig 4a).

When working with body waves it is logical to constrain the above azimuth solution by taking into account observed arrival time differences. For a specific event location this parameter defines a curve in geographic space. We may assume that the associated probability density function is represented by a Gaussian surface along the curves of constant arrival time differences which may be considered to be parallel straight lines.

Using the notations $f(x,y)$ and $g(x,y)$ for the azimuth and time difference probability distributions, it is possible to determine the epicenter or the point of maximum likelihood by forming the product

$$F(x,y) = f(x,y) \cdot g(x,y) \qquad (1)$$

and then differentiating.

However, we want to proceed in a slightly different way by introducing a method which is more convenient for programming. Suppose that we have obtained a Gaussian probability density $f(x,y)$ based on simulated azimuth data for a given region. Furthermore, assuming the arrival time differences to be normally distributed, the function $g(x,y)$ constitute a "Gaussian ridge" along the lines of constant time differences. In real case, the azimuth observations give a preliminary epicenter location P while the P-travel time difference defines a line $\underline{l}$ (see Fig 3a). In general the line $\underline{l}$ does not

plane through the line $\underline{n}$ and perpendicular to the xy-plane (see Fig 3b). The standard deviations of the two distributions in this particular direction are easily calculated and by finding the maximum of the product $F(\eta) = f(\eta) \cdot g(\eta)$, the distance d of the point of maximum likelihood from P may be shown to be:

$$d = \frac{\sigma_f \cdot \eta_o}{\sigma_f + \sigma_g} \qquad (2)$$

where σ_f and σ_g are the standard deviations of f(x,y) and g(x,y) along the line $\underline{n}$, and η_o is the separation between the points P and M (see Fig 3b). The two array epicenter location methods are demonstrated in Fig 4, using the data simulation approach outlined in the previous section. The above procedure will be especially effective in case the confidence ellipse has a considerable eccentricity and the time difference line is nearly parallel to the shortest axis, e.g. when the two azimuth lines intersect under a very sharp angle.

Seismicity and Epicenter Location

As it is well known, earthquake occurence is closely associated with typical geomorphical features like mountain chains, island arc systems and oceanic ridges. In many regions the seismicity area is shaped like a narrow band and this information may in such cases be used for further constraining the event location solution based on one or two arrays. Mathematically the prolonged seismicity area may be represented by the equation of its center line and

above event data did not include variances of the DT/DΔ and azimuth parameters, reasonable estimates of the associated 95% confidence ellipses have been obtained by the simulation approach discussed previously - and are included in the figures. A few comments to the presented results are as follow: Due to its larger aperture LASA is expected to have a better location performance than NORSAR, and this is in fact observed (Fig 6 and 7). The preliminary location calibration vectors in use at NORSAR seem to be troubled by small systematic errors, and an azimuth bias of 1 deg was introduced in case of the Kurile Islands events (see Fig 7). Even better epicenter locations should be obtainable if absolute travel time corrections for the two arrays were available. Another factor of some importance is the shape of the azimuth confidence ellipse as the intersection between this and the line of constant time difference determines the final solution. As mentioned above estimates of azimuth variances were not available to us. This problem is clearly demonstrated in Fig 8 when using seismicity information for improving event locations. Altogether 11 events on the Mid-Atlantic Ridge were analysed, and the results are presented in Table 4. NORSAR's location performance in this region is not impressive, but some improvements were gained by introducing seismicity. This is partly due to small intersection angles between the seismicity line and observed azimuth values. Another source of location errors is the relatively poor DT/DΔ estimates due to the complicated P-signals from earthquakes in the Mid-Atlantic Ridge region.

tions on the subarray level were computed in the ordinary way, i.e., taking the average of the difference between observed and predicted arrival times across the array and formulated as:

$$\Delta T_{ij} = (TO_{ij} - \overline{TO}_j) - (TT_{ij} - \overline{TT}_j) \qquad (3)$$

where TO_{ij} and TT_{ij} are observed and predicted travel times at the i-th subarray for the j-th event. The average values $\overline{TO}_j$ and $\overline{TT}_j$ are included in eq. (3) as we used the center of gravity of the available subarrays as a reference point. During the NORSAR interim operation the center subarray 01A was inactive.

The results obtained, are displayed in Fig 9. We have also performed a quantitive "trend" check of the station correction data. The idea is that a possible time delay response of heterogeneous structures in the crust and the uppermost part of the mantle should result in a certain pattern in the subarray time anomalies across the array. We have here followed a procedure described by Larner (1969). It consists essentially in projecting the subarrays into a plane which final orientation is that direction where the time anomalies vary most smoothly in a least squares sense. The azimuth of the trend plane is perpendicular to the projection plane and is indicated on Fig 9. It should be noted that we found the same trend direction of around 130° for the individual events with very few exceptions. In the latter case the orientation was around 50° and typical for a few small areas like one south of Hokkaido. In short, the one-dimensional model for subarray station time delays for NORSAR as shown in Fig 9, is considered acceptable as a first order approximation for simulating biased location errors. It is beyond the scope of the paper to discuss the geologic structures in the NORSAR area in any detail.

value of the mislocation vector and hence its gradient are relatively large especially in view of NORSAR's array diameter of around 110 km. In practice, this means that in order to avoid excessive errors in event locations based on a single array like NORSAR extensive calibration files are part of its software system. However, for epicentral distances beyond 85 deg and including most of the core shadow zone, where the gradients of the slowness curves are small, large mislocations are likely to occur, unless secondary arrivals, seismicity or external information are available. Finally, it should be noted that NORSAR observed velocity or $DT/D\Delta$ values are not easily interpreted in terms of heterogeneities in the mantle due to the large bias in the original data. The same seems to be valid for the LASA array according to Iyer (1971).

DISCUSSION

The simulation of one array location capabilities on the computer is straight forward as demonstrated previously. An interesting feature is how the small velocity anomaly at $\Delta \sim 30$ deg effects the accuracy of the epicenter coordinates in the corresponding distance range (see Fig 2). Moreover, experience gained in NORSAR event analysis indicates that complicated and high-frequency P-signals often give poor slowness and henceforth distance estimates. For example, earthquakes in the Greece - Turkey region are problematic as the computed epicentral distances, without analyst overriding the solution, may be 10 to 20 deg wrong, while the corresponding azimuth estimates remain reliable. An explanation for pecularities of the above kind besides complicated upper mantle structures, is that the P-waves

relative precise event locations. The significance of the presented one-dimentional model for time delays across NORSAR (fig 9) is that heterogeneous structures in the site and source regions tend to mask smaller anomalies in the earth's interior. One way to circumvent this problem may be to utilize, say PcP phases for calibrating core phases having the same azimuth. (Felix and Engdahl, 1971). An other alternative is to compare slowness values between separate branches of say, core waves as demonstrated by Doornbos and Husebye (1972).

Finally, we should like to remark that simulating event location capabilities of seismic arrays on the computer represents a valuable tool for handling problems of this kind as a minimum of observational data is required. Moreover, the simulation approach gives an estimate of expected precision in the epicenter solution, and thus facilitate identification of possible biased observational errors.

Acknowledgements

Mr. K.A. Berteussen assisted in the subarray time delay measurements, and his help is greatly appreciated.

Iyer, H.M., Variation of apparent velocity of teleseismic P-waves across the Large-Aperture Seismic Array, Montana, J. Geophys. Res., 76, 8554-8567, 1971.

Kanestrøm, R. and Haugland, K., Crustal structure in southeastern Norway from seismic refraction measurements, Sci. Rep. No 5, Seismological Observatory, Univ. of Bergen, 1971.

Larner, K., Near Receiver scattering of teleseismic body waves in layered crust-mantle models having irregular interfaces, Ph. D. thesis, Mass. Inst. Tech., 1969.

Mack, H., Nature of short-period P-wave signal variations at LASA, J. Geophys. Res., 74, 3161-3170, 1969.

Table 4 : The NOAA focal parameters for earthquakes in the Mid-Atlantic region used in analysis of seismicity information for improving epicenter locations (see also Fig 8). The NOAA focal parameters and NORSAR first and final (columns NORSAR P and F) event locations are included. The columns DDP and DDF give the distance between the NOAA solution and the first and final NORSAR location. The EPIM column gives the distances the epicenter was moved when seismicity was taken into account.

Figure 7 : NORSAR and LASA epicenter locations for 9 earthquakes in the Kurile Islands region compared to those of NOAA. A biased error in azimuth of 1.0 deg seems to occur in the NORSAR data. The open and closed rings indicate biased and unbiased observations. The given 95% confidence ellipses are based on standard deviations of 0.5 deg in azimuths and 2.0 sec in arrival times.

Figure 8 : Seismicity information utilized for improving epicenter locations in the Mid-Atlantic ridge area (events no 2 and 5 in Table 4).

Figure 9 : In the a-figure the relative time delays for 18 individual NORSAR subarrays, and these values are used in the biased error location model. In the b-figure the same time delays are also plotted as a function of NORSAR subarray configuration. The MOHO depth contours are taken from a paper by Kanestrøm and Haugland (1971).

Figure 10 : Observed and simulated biased observational errors in slowness and azimuth for the NORSAR array.

NO	DATE m/d/y	O.TIME h/m/s	T_N-T_L sec	MAG M_b	D km	NOAA lat	NOAA long	LASA lat	LASA long	NORSAR lat	NORSAR long	AZIMUTH lat	AZIMUTH long	AZIMUTH&TIME lat	AZIMUTH&TIME long
1	06/06/71	10/38/05	252.5	4.1	35	8.6N	79.3W	10N	78W	10.7N	76.1W	8.8N	77.3W	10.2N	78.2W
2	06/12/71	19/18/48	162.0	5.0	43	18.9N	64.3W	19N	65W	22.8N	63.4W	19.7N	65.6W	19.3N	64.5W
3	07/08/71	05/54/12	194.0	5.0	48	19.1N	68.0W	18N	69W	23.2N	67.1W	19.2N	69.9W	18.5N	68.8W
4	08/27/71	06/37/53	193.1	4.7	33	19.2N	68.1W	18N	69W	23.2N	67.2W	19.2N	69.9W	18.5N	68.7W
5	09/13/71	09/00/26	203.4	4.7	44	6.9N	71.8W	7N	72W	6.4N	72.7W	7.4N	72.2W	7.2N	72.5W
6	09/21/71	20/31/09	208.5	4.8	150	6.8N	73.1W	6N	73W	7.7N	72.5W	6.6N	73.3W	6.3N	73.1W
7	09/30/71	20/27/58	161.2	4.9	152	18.1N	64.5W	17N	65W	20.0N	63.9W	17.7N	65.5W	17.2N	64.7W
8	11/15/71	00/02/09	208.7	4.8	164	6.8N	73.1W	6N	72W	8.6N	71.3W	6.9N	72.4W	7.2N	72.7W
9	11/22/71	04/55/00	202.9	4.8	36	8.8N	71.2W	8N	72W	10.4N	69.1W	6.9N	71.3W	7.4N	71.7W
10	11/25/71	11/12/25	209.7	5.1	159	6.8N	73.0W	6N	73W	8.9N	71.0W	5.9N	72.9W	6.2N	73.2W
11	12/23/71	00/08/50	132.2	4.8	16	14.6N	60.9W	14N	61W	17.8N	58.9W	14.3N	61.1W	14.2N	61.0W
12	12/23/71	13/17/08	135.0	4.7	170	15.1N	61.4W	13N	61W	14.2N	62.4W	14.6N	62.3W	14.2N	61.6W
13	12/30/71	05/00/13	226.7	4.9	43	5.6N	77.7W	6N	74W	6.4N	78.0W	10.0N	76.2W	9.0N	75.4W
14	01/03/72	07/25/23	143.3	5.0	67	10.7N	62.7W	11N	62W	12.7N	60.6W	10.9N	61.8W	11.2N	62.4W
15	01/20/72	16/31/47	239.3	4.5	82	6.7N	75.6W	7N	74W	9.0N	73.6W	7.8N	74.4W	9.8N	76.0W

Table 2

NO	DATE m/d/y	O. TIME h/m/s	MAG M_b	D Km	NOAA lat	NOAA long	NORSAR P lat	NORSAR P long	NORSAR F lat	NORSAR F long	DDP Km	DDF Km	EPIM Km
1	04/30/71	03/15/35	4.7	33	11.4S	12.8W	3.6 S	7.0W	2.4 S	9.9W	1073	1045	343
2	05/31/71	08/17/15	5.0	23	23.8N	45.0W	23.7 N	43.3W	23.9 N	44.8W	173	19	155
3	06/10/71	21/32/38	4.9	33	59.3N	30.4W	59.7 N	33.3W	60.3 N	30.6W	172	80	92
4	06/10/71	23/44/38	4.3	33	60.0N	30.5W	55.9 N	30.3W	55.4 N	34.2W	453	391	140
5	07/02/71	03/35/38	4.7	33	35.3N	36.3W	32.7 N	37.5W	33.8 N	37.9W	302	215	122
6	07/11/71	05/30/53	5.1	33	0.9S	13.3W	2.0 N	9.6W	1.8 S	11.1W	519	261	447
7	08/03/71	05/34/26	5.0	33	28.3N	39.2W	31.2 N	37.1N	32.8 N	37.6W	382	521	182
8	08/03/71	20/59/29	4.7	33	29.4N	39.3W	34.7 N	34.3W	35.6 N	39.7W	844	911	101
9	08/05/71	01/58/51	6.3	33	0.9S	22.1W	1.3 N	17.9W	0.3 N	18.0W	527	477	177
10	08/12/71	01/25/53	4.2	33	23.9N	45.7W	27.4 N	42.1W	27.8 N	44.1W	537	464	202
11	09/08/71	20/32/29	4.9	33	53.8N	35.3W	54.7 N	33.3W	55.4 N	34.5W	163	182	113
12	09/14/71	19/53/14	5.2	33	0.8N	29.0W	2.4 N	26.0W	0.5 N	26.3W	374	315	217
13	09/22/71	06/29/49	4.8	33	31.1N	41.6N	35.3 N	38.8W	33.6 N	38.2W	539	429	195

Table 4

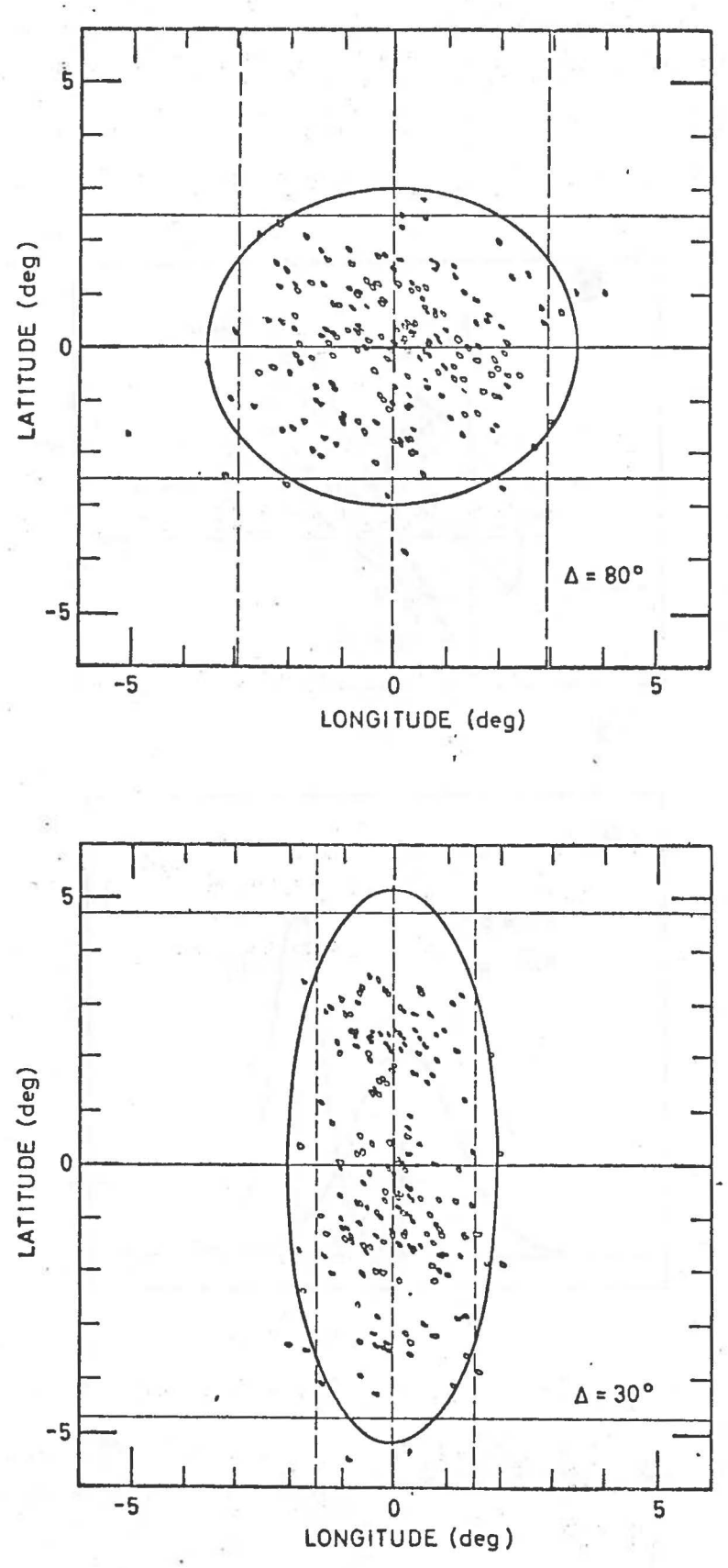
5
0
-5
LATITUDE (deg)
-5
0
5
LONGITUDE (deg)
Δ = 80°
5
0
-5
LATITUDE (deg)
-5
0
5
LONGITUDE (deg)
Δ = 30°

Fig. 2

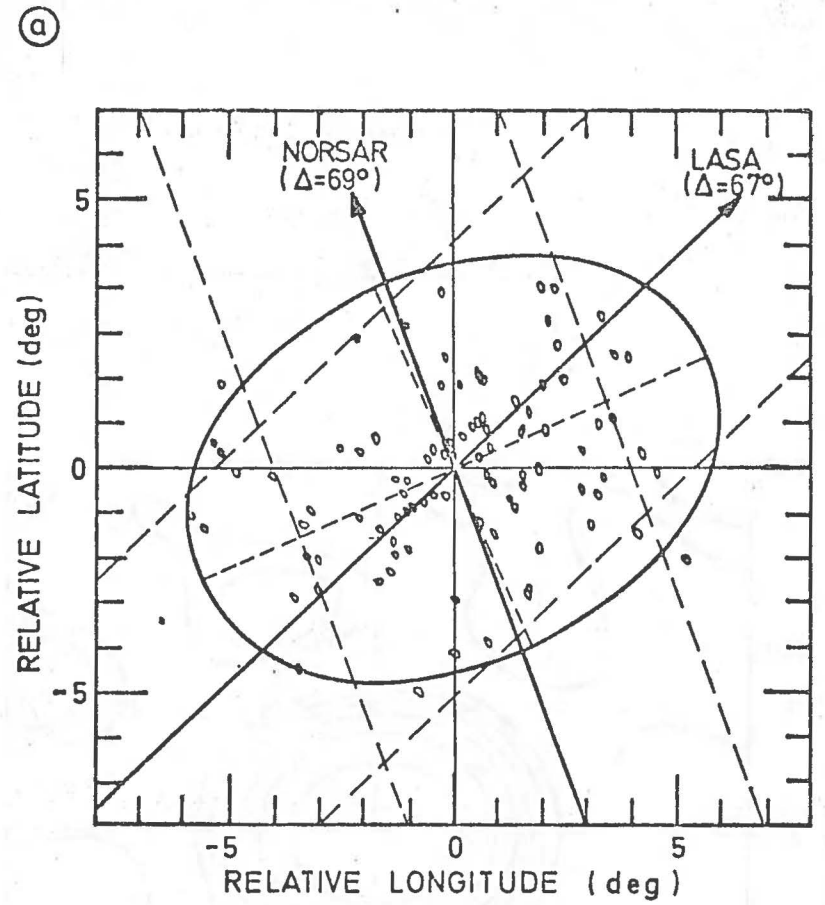
(a)
NORSAR
(Δ=69°)
LASA
(Δ=67°)
5
0
-5
RELATIVE LATITUDE (deg)
-5
0
5
RELATIVE LONGITUDE (deg)

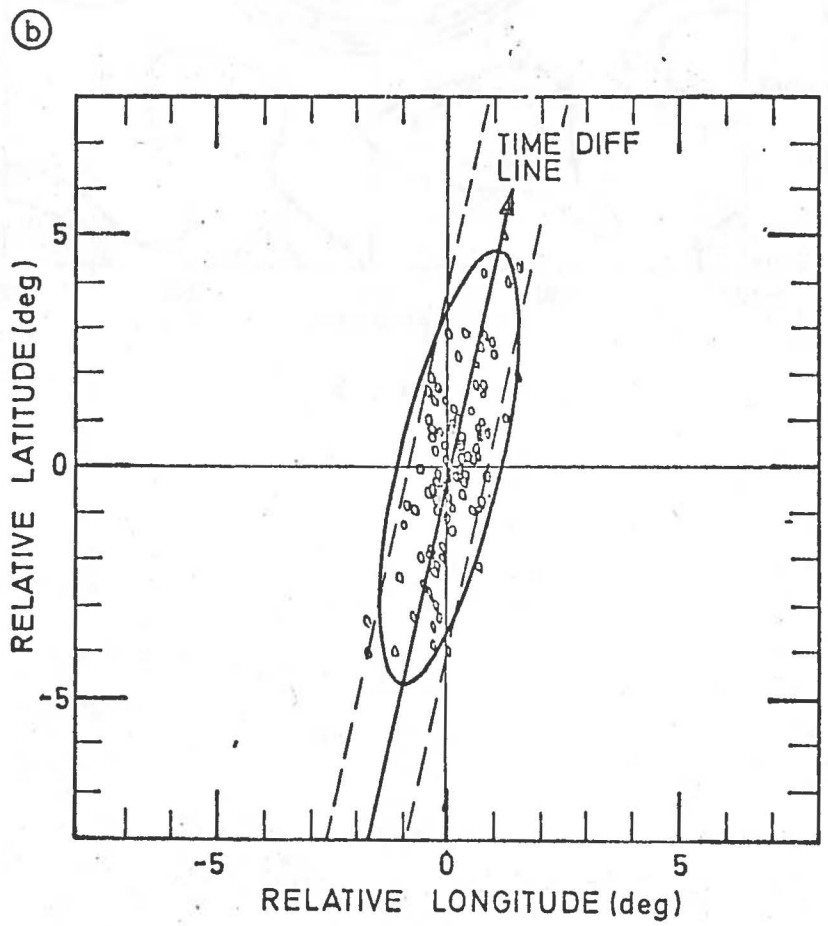
(b)
TIME DIFF
LINE
5
0
-5
RELATIVE LATITUDE (deg)
-5
0
5
RELATIVE LONGITUDE (deg)

Fig. 4

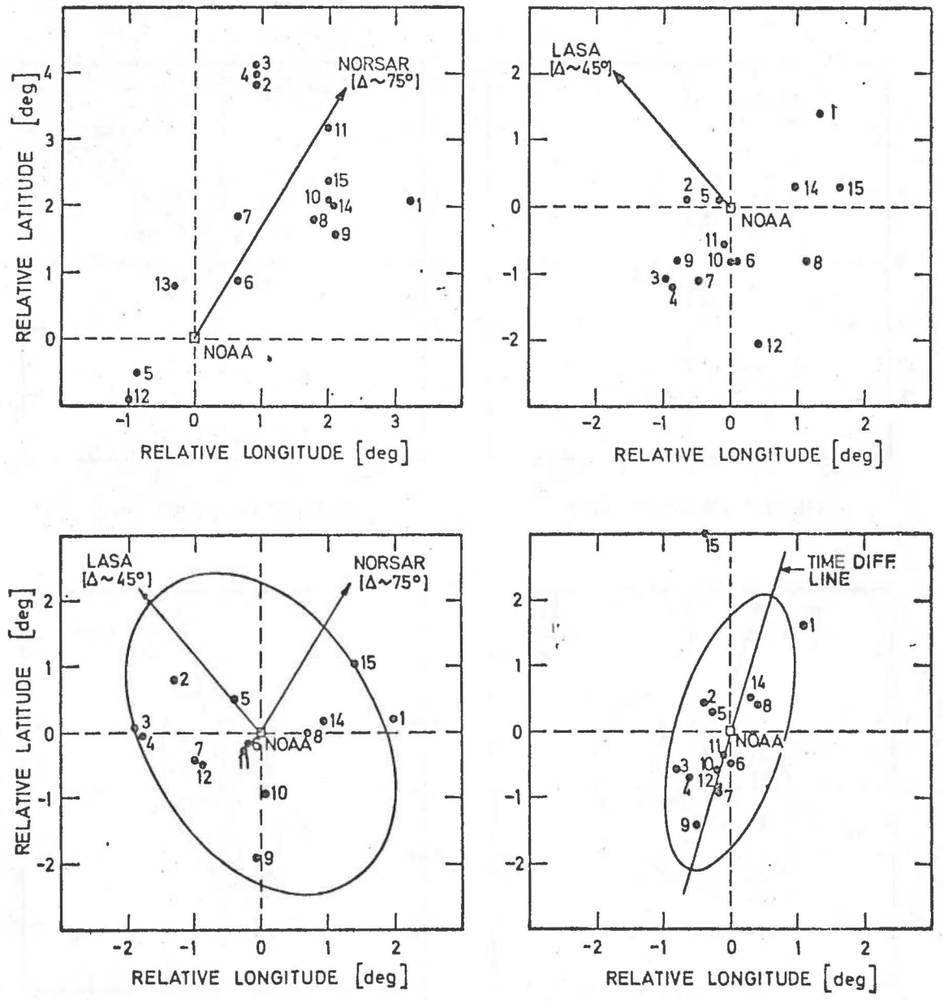
NORSAR
[Δ~75°]
LASA
[Δ~45°]
NOAA
RELATIVE LATITUDE [deg]
RELATIVE LONGITUDE [deg]
TIME DIFF.
LINE

Fig. 6

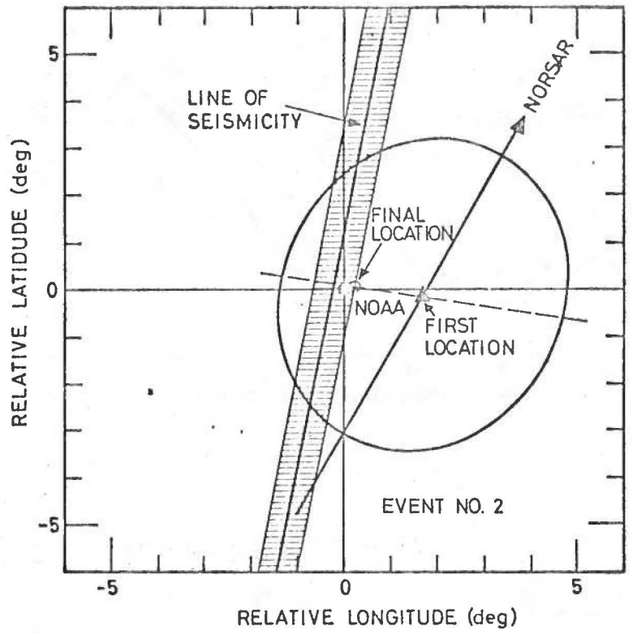
LINE OF
SEISMICITY
NORSAR
FINAL
LOCATION
NOAA
FIRST
LOCATION
EVENT NO. 2
RELATIVE LATIDUDE (deg)
RELATIVE LONGITUDE (deg)
5
0
-5
-5
0
5

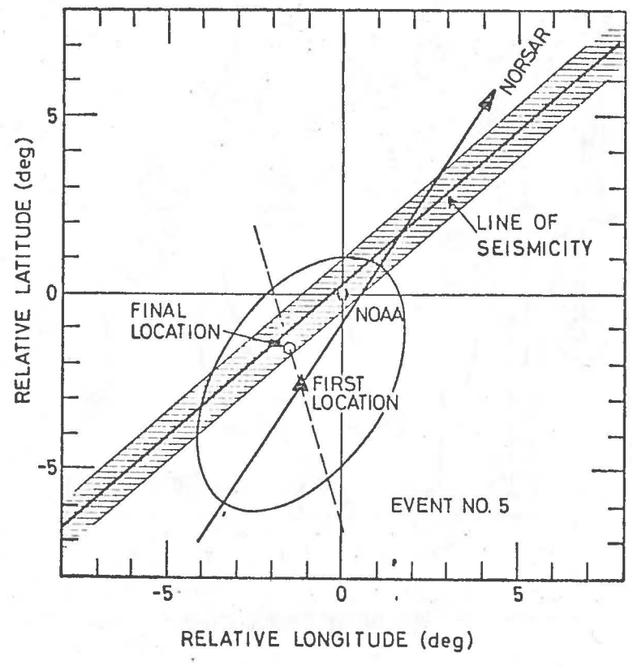
NORSAR
LINE OF
SEISMICITY
FINAL
LOCATION
NOAA
FIRST
LOCATION
EVENT NO. 5
RELATIVE LATITUDE (deg)
RELATIVE LONGITUDE (deg)
5
0
-5
-5
0
5

Fig. 8

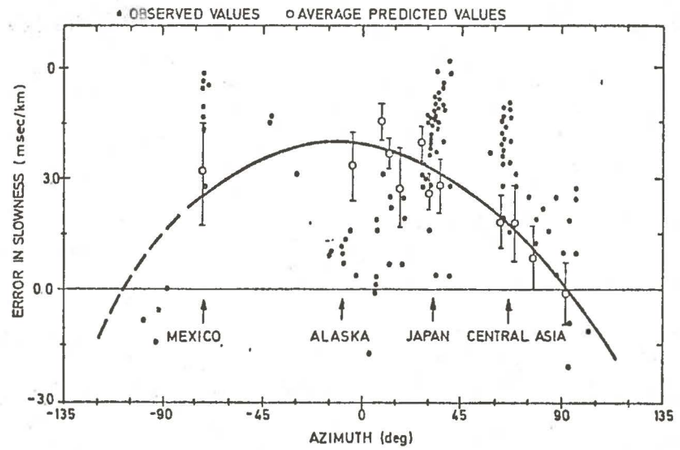
• OBSERVED VALUES o AVERAGE PREDICTED VALUES
ERROR IN SLOWNESS (msec/km)
0
3.0
0.0
-3.0
MEXICO
ALASKA
JAPAN
CENTRAL ASIA
-135
-90
-45
0
45
90
135
AZIMUTH (deg)

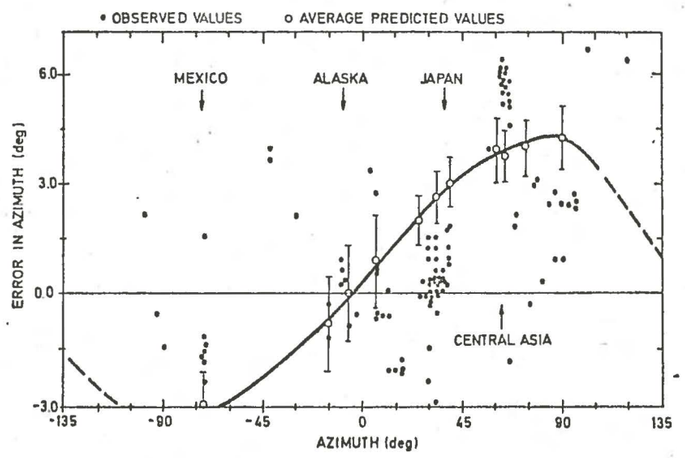
• OBSERVED VALUES o AVERAGE PREDICTED VALUES
ERROR IN AZIMUTH (deg)
6.0
3.0
0.0
-3.0
MEXICO
ALASKA
JAPAN
CENTRAL ASIA
-135
-90
-45
0
45
90
135
AZIMUTH (deg)

Fig. 10